А С Т Р О Ф И З И К А

ТОМ 65 АВГУСТ, 2022 ВЫПУСК 3

DOI: 10.54503/0571-7132-2022.65.3-429

WASP-18b SECONDARY ECLIPSES REVISITED USING TESS OBSERVATION

M.EFTEKHAR

Received 24 February 2022
Accepted 8 August 2022

We report the characterization of a transiting hot Jupiter WASP-18b at optical wavelengths measured by the transiting exoplanet survey satellite (TESS). We analyze the publicly available data collected by the TESS in sector 2. Here, we model the systematic noise using Gaussian processes (GPs) and fit it to the data using the Markov Chain Monte Carlo (MCMC) method. Modelling the TESS light curve returns a planet-to-star radius ratio, $p = 0.098010^{+0.000368}_{-0.000346}$ and secondary eclipse depth of 354^{+11}_{-10} part-per-million (ppm). The transit ephemeris of WASP-18b is updated using the MCMC method. Finally, we use updated ephemeris to look for transit time variations (TTVs) for WASP-18b to complement our study. We find a quite small deviation of transit timings from a linear ephemeris, which is statistically insignificant.

Keywords: *planetary systems: stars: individual: WASP-18: techniques: photometric: methods: data analysis*

1. *Introduction*. Exoplanet research has entered a new phase after the first finding of a hot Jupiter beyond our solar system [1] and now thousands of planets have been discovered and confirmed to date. Successful ground surveys, like as HATnet [2], SuperWASP [3], KELT [4,5], NGTS [6] have discovered the majority of giant planets. Several pioneering photometric transits searches with spacebased platforms have been made so far including CoRoT [7], Kepler [8], K2 [9] and TESS [10] which these efforts have increased the number of discovered exoplanets.

Since August 2018, the TESS mission [10] has been delivering high-precision photometric observations in a broad optical band (0.6-0.95 μm) for a large sample of bright stars from the southern and northern hemispheres. TESS has detected thousands of planet candidates and planets that have been discovered and confirmed to date. The recorded light curves have provided us with a trove of knowledge on exoplanet systems [11].

WASP-18bA was discovered by Hellier et al. [12]. Because of its short orbital period of ~0.941 days, bright host F6-type star ($V = 9.3$) and inflated radius ($a/R_s = 3.442$, $R_p = 1.165 R_J$) makes it one of the best targets for investigating the secondary eclipse depth and ephemeris. The relative brightness of the companion's dayside hemisphere determines the depth of the secondary eclipse. The primary transit (when an exoplanet passes in front of its host star) and the depth of the secondary eclipse of WASP-18b have been measured in several studies (i.e., when an exoplanet is occulted by its host star). The planet-to-star radius ratio and eclipse depth of WASP-18b were measured to $0.09716^{+0.00014}_{-0.00013}$ and 341^{+17}_{-18} ppm respectively, in the TESS bandpass [13].

Because of the WASP-18b short orbital period is thought to be tidally locked to its host star and the planet's rotation to be synchronized with the orbit [14]. Massive exoplanets in tight orbits must decay according to tidal dissipation within their host stars, according to theoretical calculations and observations [15]. We can learn more about this orbital evolution by studying precise transit timing. We're looking for short-term TTVs in the sector 2 that might suggest the presence of a third body in this system as part of our research. Furthermore, stellar activity features in photometric observations might impact planetary parameters. Anomalies in transit light curves can be caused by stellar activity features and transiting planets, resulting in inaccurate transit duration, timing, and depth measurements. These uncertainties also might potentially have an impact on the calculation of parameters such as planet radius [16].

In this work, we model primary transits and secondary eclipses of WASP-18b. We extend our study by using our revised ephemeris to search for WASP-18b TTVs. Dealing with and mitigating stellar noise is one of the most difficult aspects of measuring low-amplitude exoplanetary signals. To achieve this, we focus on the GP method for modelling correlated noise. The paper is organized as follows; in Section 2, we describe the TESS observations, data preparation techniques, and our approach to account for correlated noise to prepare the light curves for fits. We discuss our selection model for primary transit, secondary eclipse, the regression analysis, and TTV in detail in Section 3. In Section 4, we summarize our results from this study.

2. *Observation*. WASP-18bA was monitored by TESS with the two minute cadence mode in Sector 2, included in the list of preselected target stars using a 11×11 pixel subarray centered on the target. the raw images were reduced using the science processing operations Center (SPOC) pipeline [17], which was developed at NASA Ames Research Center based on the Kepler mission science pipeline. For the results presented in this paper, we decided to use Presearch Data Conditioning (PDC) light curves because they are corrected systematic and dilution effects. PDC data is also cleaner than simple aperture photometry light curves (SAP) and show significantly less reduced scatter and short-timescale flux variations [18,19].

The data were normalized using the median of the PDCSAP light curve. We corrected the PDCSAP light curve further for the remaining systematic, even though the dominating systematic were corrected by default. To do so, we smoothed the PDCSAP light curve using the median detrending technique with a window length of one orbital period, keeping variability at the planetary period of the WASP-18b light curve. These regressions were implemented using the Python package wotan as shown in Fig.1 [20]. These reprocessed data are taken into account in our subsequent analyses.

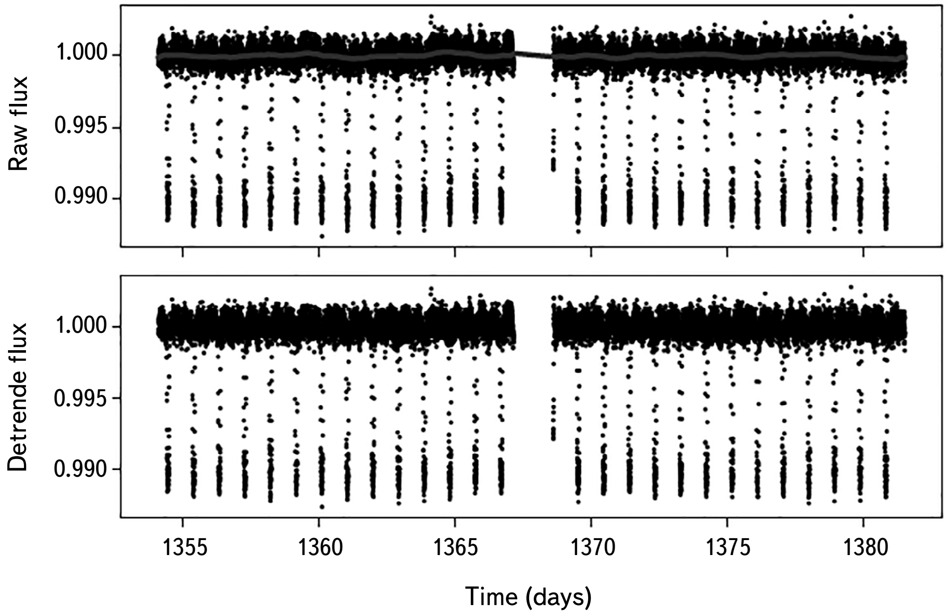

Fig.1. (Top) WASP-18's TESS light curve (PDCSAP flux). The trend generated by applying a detrending filter determined by wotan is shown by the solid line, while the PDCSAP photometry is represented by dots. (Bottom) PDCSAP light curve after median detrending normalization.

3. *Analysis.*

3.1. *Primary transit modeling.* We utilized the publicly available software *Juliet* [21] to compute all the planetary parameters in this study. *Juliet* allows us to model the transit by *batman* package [22]. Rather than modeling systematic errors as a deterministic function with auxiliary measurement parameters, the Gaussian process (GP) presents a nonparametric approach to modeling systematic errors from the photometry data. GPs aim to model the likelihood, L, as though it came from a multi-variate gaussian distribution, that is,

$$\ln\mathcal{L} = -\frac{1}{2}\left[N\ln 2\pi + \ln\left|\sum\right| + \vec{r}^{\,T}\sum^{-1}\vec{r}\right]. \qquad (1)$$

Here, $\ln\mathcal{L}$, is the log-likelihood, N shows the number of datapoints, the covariance matrix is Σ and the vector of the residuals is $\vec{r}$. A GP uses so-called kernels to determine the structure of the covariance matrix and provide a form for it (see [21] for a detailed technical description). In our study, we employed the Matérn-3/2 kernel using the *celerite* package [23] to diagnose instrumental systematic errors in TESS photometry data. *Celerite* speeds up the posterior sampling within *Juliet* by making the log-likelihood computation blazing fast. The correlation kernel, which was aimed to capture the systematic variation of the data (see [20]), formulated as:

$$K_{i,j}(\tau) = \sigma_{GP}^2\left(1+\frac{\sqrt{3}\tau}{\rho_{GP}}\right)\exp\left(-\frac{\sqrt{3}\tau}{\rho_{GP}}\right). \tag{2}$$

Here τ is the time lag, σ_{GP} is the covariance amplitude and ρ_{GP}, is the correlation timescale of the GP.

We employed gaussian priors for the orbital period, P, and mid-transit time,

Table 1

PRIOR SETTINGS AND THE BEST-FIT VALUES ALONG WITH THE 68% CONFIDENCE INTERVALS IN THE PRIMARY TRANSIT FIT FOR WASP-18b. DERIVED PHYSICAL PARAMETERS FROM JOINT FIT FOR WASP-18b ARE SHOWN IN THE BOTTOM PANEL

Parameters	Symbol	Prior	Value
Orbital period(days)	P	$\mathcal{N}(1.21749,\ 0.1)$	$0.9414550^{+0.0000039}_{-0.0000039}$
Mid-transit time(days)	T_0	$\mathcal{N}(1765.5338,\ 0.1)$	$1354.457881^{+0.000059}_{-0.000059}$
Parametrization for p and b	r_1	$\mathcal{U}(0,\ 1)$	$0.592952^{+0.017463}_{-0.015453}$
Parametrization for p and b	r_2	$\mathcal{U}(0,\ 1)$	$0.098010^{+0.000368}_{-0.000346}$
Limb-darkening parameter	q_1	$\mathcal{U}(0,\ 1)$	$0.214^{+0.045}_{-0.041}$
Limb-darkening parameter	q_2	$\mathcal{U}(0,\ 1)$	$0.271^{+0.063}_{-0.074}$
Orbital eccentricity	e	fix	0
Argument of periapsis (deg)	ω	fix	269
Stellar density (kgm^{-3})	ρ_s	$\mathcal{J}(100,\ 10000)$	$871.061^{+0.008}_{-0.008}$
Dilution factor	DTESS	fixed	1
Mean out-of-transit	MTESS	$\mathcal{N}(0,\ 10^{-1})$	$-0.0000004^{+0.000004}_{-0.000004}$
Additive photometric jitter term(ppm)	σ_ω	$\mathcal{J}(10^{-6},\ 10^{-6})$	$0.01439^{+0.00087}_{-0.00088}$
Amplitude of GP (ppm)	σ_{GP}	$\mathcal{J}(10^{-6},\ 10^{6})$	$0.00046^{+0.00003}_{-0.00004}$
Matern time-scale (days)	ρ_{GP}	$\mathcal{J}(10^{-3},\ 10^{3})$	$0.07168^{+0.00602}_{-0.00661}$
Planet radius in units of stellar radius	R_p/R_s		$0.098010^{+0.000368}_{-0.000346}$
Semi-major axis in units of stellar radii	a/R_s		$3.442^{+0.017}_{-0.017}$
Impact parameter	b		$0.098010^{+0.000368}_{-0.000346}$
Inclination angle (deg)	i		$83.5^{+0.26}_{-0.28}$
Limb darkening coefficients	u_1		$0.218^{+0.028}_{-0.026}$
Limb darkening coefficients	u_2		$0.301^{+0.035}_{-0.039}$

T_0 based on [24]. Instead of fitting directly for the planet-to-star radius ratio, $p = R_p / R_s$, and the impact parameter of the orbit b, *Juliet* uses the new

Table 2

PRIOR SETTINGS AND THE BEST-FIT VALUES ALONG WITH THE 68% CONFIDENCE INTERVALS IN THE SECONDARY ECLIPSE FIT FOR WASP-18b

Parameters	Symbol	Prior	Value
Orbital period(days)	P	$\mathcal{N}(1.21749, 0.1)$	$0.941530^{+0.000079}_{-0.000056}$
Mid-eclipse time(days)	$T_{0,e}$	$\mathcal{N}(1766.74755, 0.1)$	$1354.92697^{+0.00061}_{-0.00099}$
Parametrization for p and b	r_1	$\mathcal{U}(0, 1)$	$0.57846^{+0.00087}_{-0.00087}$
Parametrization for p and b	r_2	$\mathcal{U}(0, 1)$	$0.01884^{+0.00042}_{-0.00041}$
Limb-darkening parameter	q_1	fix	0
Limb-darkening parameter	q_2	$\mathcal{U}(0, 1)$	$0.4963^{+0.0092}_{-0.0089}$
Orbital eccentricity	e	fix	0
Argument of periapsis (deg)	ω	fix	269
Stellar density (kgm^{-3})	ρ_s	$\mathcal{J}(100, 10000)$	$839.56^{+24.35}_{-23.44}$
Dilution factor	DTESS	fixed	1
Mean out-of-transit	MTESS	$\mathcal{N}(0, 10^{-1})$	$0.00000086^{+0.00000040}_{-0.00000044}$
Additive photometric jitter term (ppm)	σ_ω	$\mathcal{J}(10^{-6}, 10^{-6})$	$0.014397^{+0.000088}_{-0.000087}$
Amplitude of GP (ppm)	σ_{GP}	$\mathcal{J}(10^{-6}, 10^{6})$	$0.00046^{+0.00003}_{-0.00003}$
Matern time-scale (days)	ρ_{GP}	$\mathcal{J}(10^{-3}, 10^{3})$	$0.07162^{+0.00603}_{-0.00659}$

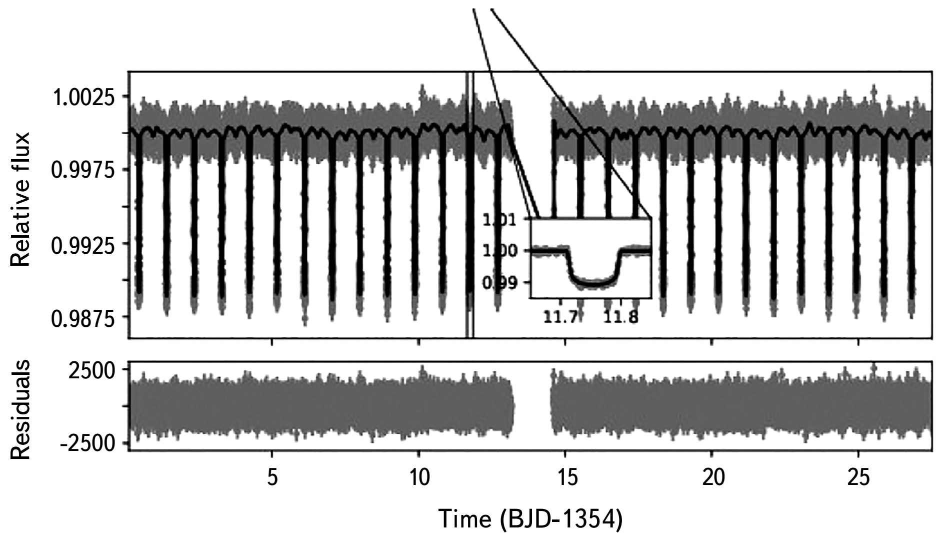

Fig.2 TESS transits of WASP-18 b. The top panels present the TESS photometry of WASP-18 as a function of time (grey points with error bars), along with the best-fit model, which consists of a transit model plus a Gaussian process (black curve) with a zoom into a single transit. The bottom panels show the corresponding residuals.

parametrization r_1 and r_2. This ensures that p and b have a whole range of physically plausible values and that the b-p plane is sampled uniformly (see [25], for details). In addition, instead of using individual a/R_s values, we can fit for stellar density, ρ_s for all transiting planets in the system, as shown in Table 1 and 2. For our data, we consider a quadratic limb darkening law with a uniform prior of 0 to 1 on both parametrs q_1 and q_2 [26]. We fixed the dilution factor to one because we used TESS's PDCSAP (which should have been corrected for light dilution in principle). The eccentricity, e, is also fixed to zero and set non-informative log-uniform prior to stellar density. We fit the instrumental jitter term to account for additional systematic and the outof-transit flux. *Juliet* predicts the model on the full time-series (see [21] for a detailed technical description). Fig.2 presents reprocessed TESS light curve of WASP-18b as well as the the full median posterior model (i.e., the deterministic part of the model plus the median GP process). The Fig.3 shows the zoom of the phase-folded light curve and the best-fit model.

Using the dynamic nested sampling approach implemented in dynesty [27,28], we determine the posterior probability distribution of the system parameters. The

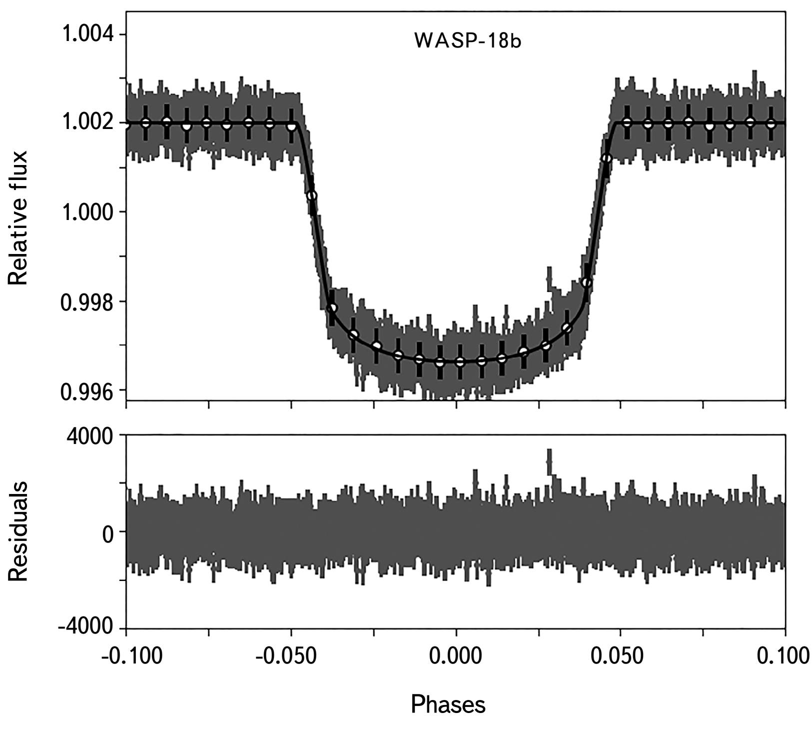

Fig.3. Phase-folded light curve presented as grey points showing the primary transit. The binned data (hollow black circle) are over plotted and the best-fitted model (black lines). In the bottom panel, the corresponding residuals are presented.

median and 1σ uncertainties derived from the posterior distributions of our analysis are listed in Table 1. Fig.4 also shows the corner plot for our obtained posterior distributions from the transit.

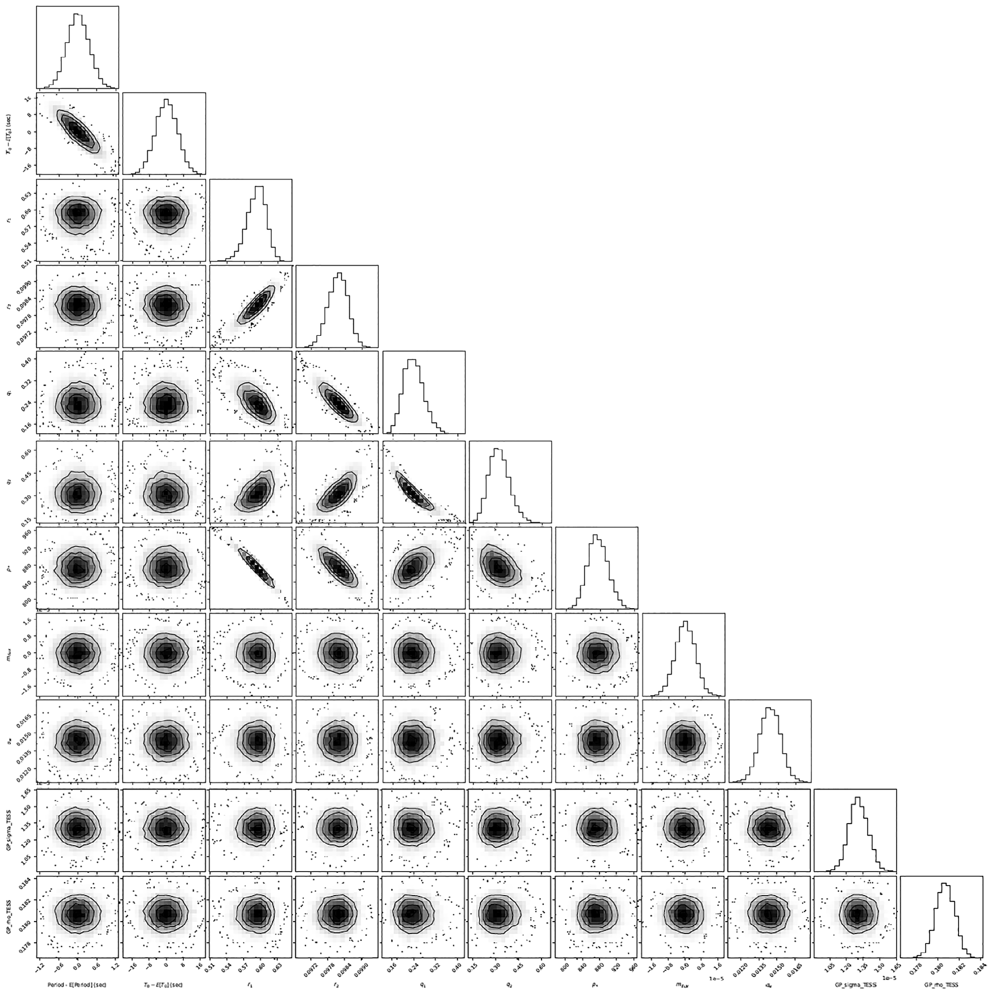

Fig.4. Retrieved posterior distributions obtained from our fitting model to the primary transit of the WASP-18b.

3.2. *Secondary eclipse modeling*. Both our transit and eclipse models by *batman*. The mid-secondary eclipse time for WASP-18b is calculated using the mid-transit time, assuming a circular orbit. The secondary eclipse model is based on the same orbital parameters as the primary transit 3.1. So, all parameters are coupled to the values of the primary transit, except for limb darkening, which fixes q_1 to zero, because limb darkening has no effect on the secondary eclipse

[29]. Our reprocessed data, as well as the best-fitted WASP-18b model, are shown in Fig.5. The results of secondary eclipse model fitting are shown in Table 2 and The corner plot for our retrieved posterior distributions from the secondary eclipse fit is shown in Fig.6.

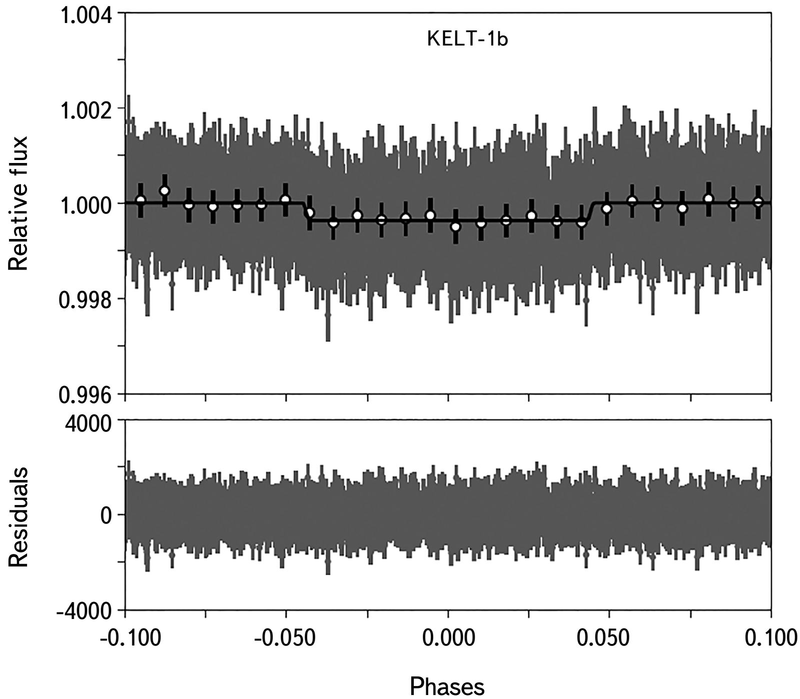

Fig.5. Phase-folded light curve is presented as grey points showing the secondary eclipse around phase 0, 0.1. The binned data (hollow black circle) are over plotted and the bestfitted model (black lines). Corresponding residuals are shown in the below panel.

3.3. *Transit timing variations*. TTV can be used to find new exoplanets with gravitational interactions in the system [30]. We assume periodic transit events in the reported results in Table 1, which means that the transit times are considered to be periodic. At this step, we investigate whether our target generates any TTV signatures. As a result, we directly fit an individual primary transit for each transit time T_n. Except for T_0 and P, all steps are performed and priors are determined as detailed in the previous section. We used Gaussian priors with a standard deviation of 0.1 days for each transit time. As a result, these parameters are calculated directly from each sample. This regression is performed using juliet [21]. The difference between observed-computed diagrams (O-C) of transit events is shown in Fig.7, which indicates very little TTV in the data.

We further evaluated if there was any evidence of periodicity in the measured

TTVs using the generalized Lomb-Scargle (GLS) periodogram [31]. The GLS periodogram on TTV of WASP-18b (see Fig.8), shows the value of the strongest peak in GLS periodograms is at 2.33 days, with a false alarm probability (FAP) of 0.32, which is computed as described in [31]. The strongest peak in GLS

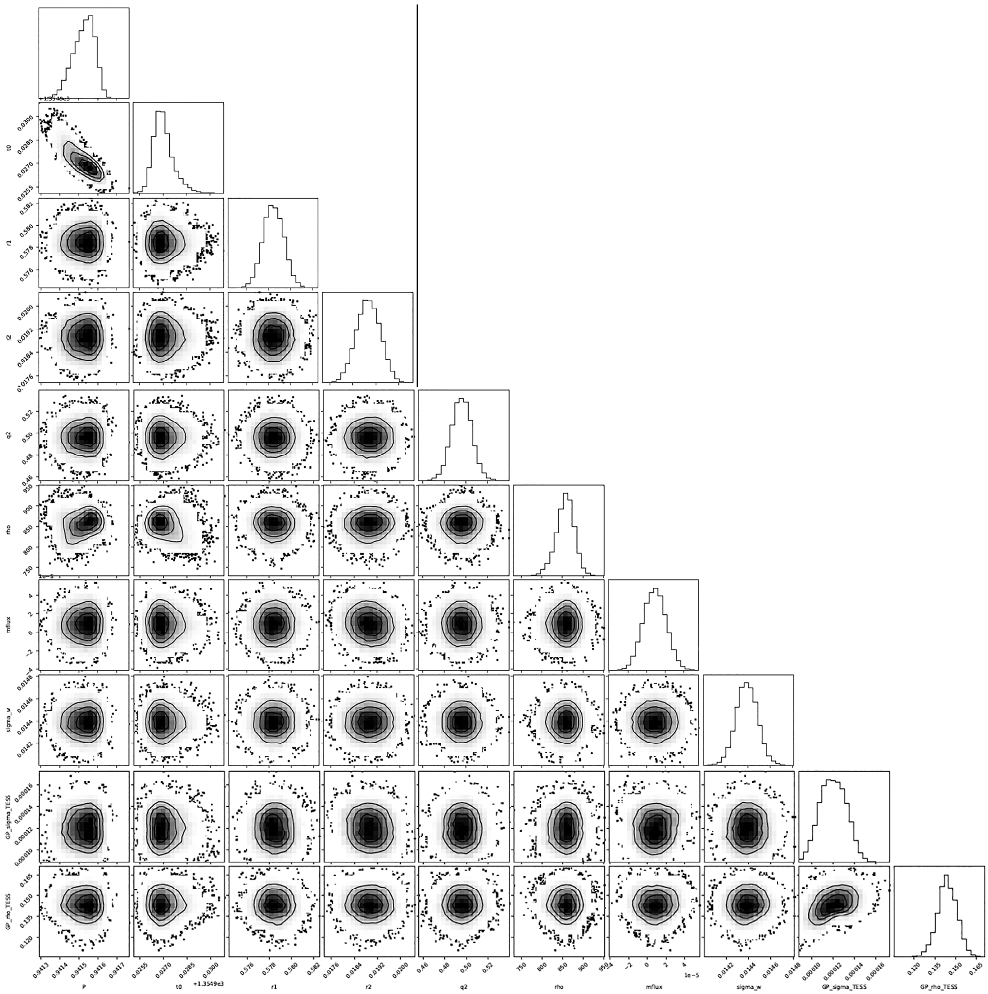

Fig.6. Retrieved posterior distributions by fitting model to the secondary eclipse of the WASP-18b.

periodograms is close to half of the stellar rotation rate for our selected host star, which is $P_{Rot} = 3.7$ days based on their values reported in [32]. This suggests that the variation we measured in TTVs is most probably caused by the imperfect elimination of stellar activity [16]. We also provide the transit times we used in our short-term timing analysis, which are listed in Table 3.

Table 3

WASP-18b TRANSIT TIMES

Transit number	Mid-transit time (BJD-2457000)	Transit number	Mid-transit time (BJD-2457000)
1	$1354.457881^{+0.000059}_{-0.000059}$	17	$1369.521202^{+0.000061}_{-0.000062}$
2	$1355.399301^{+0.000050}_{-0.000051}$	18	$1370.462812^{+0.000059}_{-0.000057}$
3	$1356.340688^{+0.000051}_{-0.000061}$	19	$1371.404052^{+0.000052}_{-0.000061}$
4	$1357.282251^{+0.000061}_{-0.000051}$	20	$1372.345307^{+0.000061}_{-0.000061}$
5	$1358.223434^{+0.000061}_{-0.000061}$	21	$1373.287269^{+0.000059}_{-0.000055}$
6	$1359.165064^{+0.000061}_{-0.000061}$	22	$1374.228134^{+0.000059}_{-0.000059}$
7	$1360.106589^{+0.000052}_{-0.000051}$	23	$1375.169742^{+0.000052}_{-0.000052}$
8	$1361.048091^{+0.000061}_{-0.000061}$	24	$1376.111251^{+0.000070}_{-0.000070}$
9	$1361.989622^{+0.000060}_{-0.000053}$	25	$1377.052627^{+0.000061}_{-0.000052}$
10	$1362.931256^{+0.000051}_{-0.000060}$	26	$1377.994410^{+0.000061}_{-0.000067}$
11	$1363.872616^{+0.000061}_{-0.000061}$	27	$1378.935689^{+0.000058}_{-0.000058}$
12	$1364.813723^{+0.000061}_{-0.000061}$	28	$1379.877156^{+0.000053}_{-0.000053}$
13	$1365.755239^{+0.000062}_{-0.000054}$	29	$1380.818880^{+0.000061}_{-0.000051}$
14	$1366.696990^{+0.000061}_{-0.000059}$		

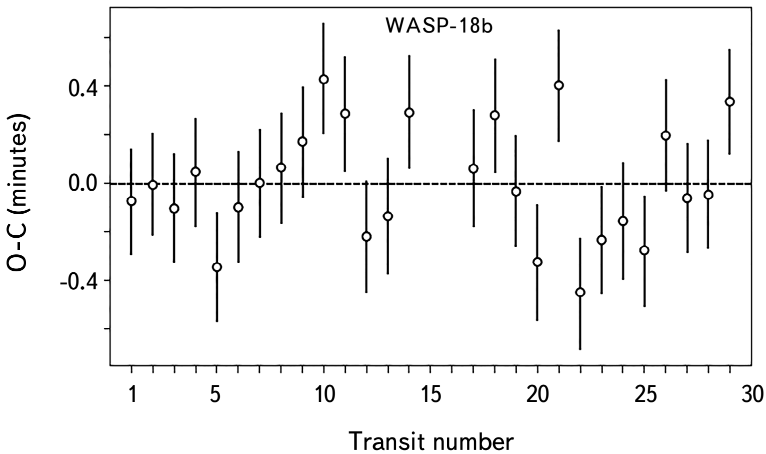

Fig.7. TTV amplitudes are calculated in minutes. The gap in the middle is caused by data downlink dead time.

4. *Summary and conclusions*. We utilize Sector 2 of TESS observations to characterize transiting ultra-hot Jupiter WASP-18b in our work. To smooth detrend the TESS data, we first applied the median detrending approach with a window length of one orbital period of WASP-18b. We did the joint fit of the GP with transits and secondary eclipses of WASP-18b. The planetary radius (in

stellar radii), (R_p/R_s), of $0.098010^{+0.000368}_{-0.000346}$, is then reliably measured by fitting a transit model to reprocessed data. We measure secondary eclipse depth with amplitudes of 354^{+11}_{-10} ppm, which is the most precise estimate for WASP-18b to date, it's also well within 1σ of the value of 341^{+17}_{-18} ppm reported in the [13] and the measured value of [11] of 339 ± 21 ppm. WASP-18b has a large secondary

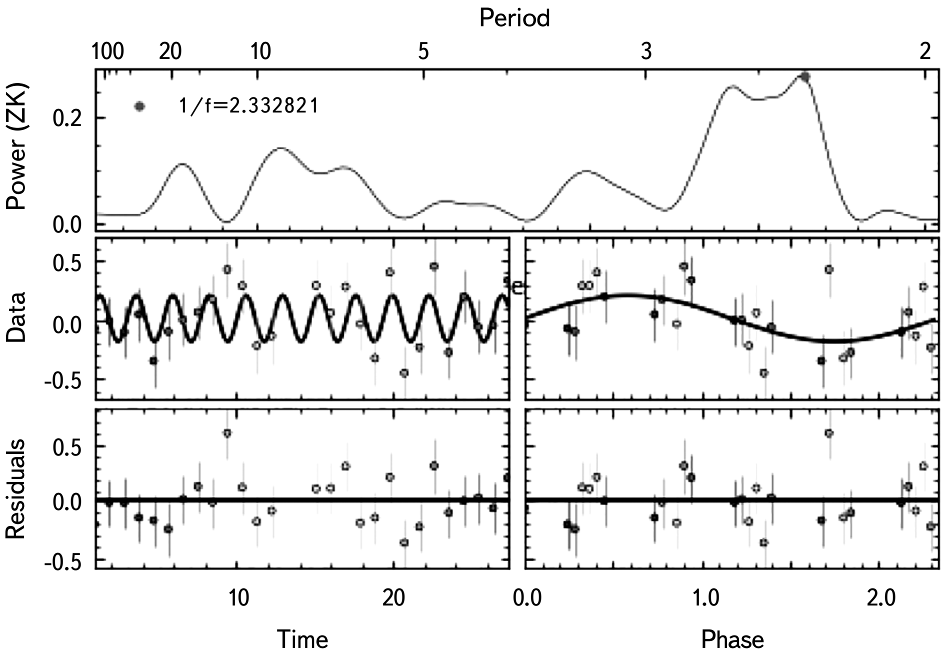

Fig.8. GLS periodogram of TTV of WASP-18b.

eclipse depth due to the combination of thermal emission and reflection in the TESS bandpass [13]. The measured values of the orbital parameters a/R_s and i of $3.442^{+0.017}_{-0.017}$ and $83.5^{+0.26}_{-0.28}$, respectively, and they are also the most precise to date and are matching the value determined by [13] within 1σ. The following equation, represented by [26], was used to estimate the limb darkening coefficients:

$$u_1 = 2\sqrt{q_1 q_2} \tag{3}$$

and

$$u_2 = \sqrt{2 q_1 (1 - 2 q_2)} \tag{4}$$

u_1 and u_2, are 0.218 and 0.301, respectively, which are comparable to the limb darkening coefficients of $u_1 = 0.219$ and $u_2 = 0.312$ given by [33]. In comparison to other published values in the literature [11,13], we find that our results are generally in good agreement.

The most notable result of our investigation is the most precise detection of WASP-18b's secondary eclipse in the TESS bandpass, as well as the robust measurement of its orbital parameters. To extend our analysis, we searched for individual transit times to see whether there were any TTVs. TTV OC diagrams (see Fig.7) were obtained, with a standard deviation of 0.96 minutes for WASP-18b, which is quite small.

Department of Physics, Faculty of Science, University of Zanjan, P. O. Box 313-45195, Zanjan, Iran, e-mail: m.eftekhar@znu.ac.ir

ВТОРИЧНЫЕ ЗАТМЕНИЯ WASP-18b, ПЕРЕСМОТРЕННЫЕ С ИСПОЛЬЗОВАНИЕМ НАБЛЮДЕНИЙ TESS

М.ЭФТЕХАР

Представлены характеристики "горячего Юпитера" WASP-18b в оптических длинах волн, измеренных спутником для исследования экзопланет TESS. Анализированы общедоступные данные, собранные TESS в секторе 2. Используя гауссовские процессы (GP), моделирован систематический шум и и проведена его подгонка к данным, используя метод Монте-Карло с цепями Маркова (MCMC). Моделирование кривой блеска TESS позволяет оценить отношение радиуса планеты к звезде $p = 0.098010^{+0.000368}_{-0.000346}$ и глубину вторичного затмения 354^{+11}_{-10} частей на миллион (ppm). Транзитные эфемериды WASP-18b обновлены с использованием метода MCMC. Обновленные эфемериды использованы для поиска изменений времени прохождения (TTV) для WASP18b. Обнаружено небольшое отклонение времени прохождения от линейной эфемериды, что статистически незначимо.

Ключевые слова: *планетные системы: звезды: WASP-18: фотометрические методы: анализ данных*

REFERENCES

1. *M.Mayor*, *D.Queloz*, Nature, **378**, 355, 1995. https://doi.org/10.1038/378355a0.
2. *G.Bakos*, *R.W.Noyes*, *Kovács et al.*, Publ. Astron. Soc. Pacif., **116**, 266, 2004. https://doi.org/10.1086/382735.
3. *D.L.Pollacco*, *I.Skillen*, *A.Collier Cameron et al.*, Publ. Astron. Soc. Pacif., **118**, 1407, 2006. https://doi.org/10.1086/508556.
4. *J.Pepper*, *R.W.Pogge*, *D.L.DePoy et al.*, Publ. Astron. Soc. Pacif., **119**, 923, 2007. https://doi.org/10.1086/521836.
5. *J.Pepper*, *R.B.Kuhn*, *R.Siverd et al.*, Publ. Astron. Soc. Pacif., **124**, 230, 2012. https://doi.org/10.1086/665044.
6. *P.J.Wheatley*, *R.G.West*, *M.R.Goad*, Mon. Not. Roy. Astron. Soc., **475**(4), 4476, 2018. https://doi.org/10.1093/mnras/stx2836.
7. ESA Special Publication, vol. 1306, 2006.
8. *W.J.Borucki*, *D.Koch*, *G.Basri et al.*, Science, **327**, 977, 2010. https://doi.org/10.1126/science.1185402.
9. *S.B.Howell*, *C.Sobeck*, *M.Haas et al.*, Publ. Astron. Soc. Pacif., **126**(938), 398, 2014. https://doi.org/10.1086/676406.
10. *G.R.Ricker*, *J.N.Winn*, *R.Vanderspek et al.*, Journal of Astronomical Telescopes, Instruments, and Systems, **1**, 014003, 2015. https://doi.org/10.1117/1.JATIS.1.1.014003.
11. *I.Wong*, *A.Shporer*, *T.Daylan et al.*, Astron. J., **160**, 155, 2020. https://doi.org/10.3847/1538-3881/ababad.
12. *C.Hellier*, *D.R.Anderson*, *Collier Cameron et al.*, Nature, **460**, 1098, 2009. https://doi.org/10.1038/nature0824510.1038/nature08245.
13. *A.Shporer*, *I.Wong*, *C.X.Huang et al.*, Astron. J., **157**(5), 178, 2019. https://doi.org/10.3847/1538-3881/ab0f96.
14. *T.Mazeh*, EAS Publ. Ser., **29**, 1, 2008. https://doi.org/10.1051/eas:0829001.
15. *G.Maciejewski*, *M.Fernández*, *F.Aceituno et al.*, Acta Astronomica, **68**, 371, 2018. https://doi.org/10.32023/0001-5237/68.4.4.
16. *M.Oshagh*, *N.C.Santos*, *I.Boisse*, Astron. Astrophys., **556**, 19, 2013. https://doi.org/10.1051/0004-6361/201321309.
17. *J.M.Jenkins*, Kepler Data Processing Handbook: Overview of the Science Operations Center. Kepler Science Document KSCI-19081-002, 2017.
18. *J.C.Smith*, *M.C.Stumpe*, *J.E.Van Cleve et al.*, Publ. Astron. Soc. Pacif., **124**, 1000, 2012. https://doi.org/10.1086/667697.
19. *M.C.Stumpe*, *J.C.Smith*, *J.H.Catanzarite et al.*, Publ. Astron. Soc. Pacif., **126**(935), 100, 2014. https://doi.org/10.1086/674989.
20. *M.Hippke*, *T.J.David*, *G.D.Mulders et al.*, Astron. J., **158**(4),143, 2019. https://doi.org/10.3847/1538-3881/ab3984.
21. *N.Espinoza*, *D.Kossakowski*, *R.Brahm*, Mon. Not. Roy. Astron. Soc., **490**, 2262, 2019. https://doi.org/10.1093/mnras/stz2688.

22. *L.Kreidberg*, Publ. Astron. Soc. Pacif., **127**, 1161, 2015. https://doi.org/10.1086/683602.
23. *D.Foreman-Mackey*, *E.Agol*, *R.Angus et al.*, Astron. J., **154**, 220, 2017. https://doi.org/10.3847/1538-3881/aa9332.
24. *C. von Essen*, *M.Mallonn*, *N.B.Cowan*, arXiv e-prints, 2006-09750, 2020.
25. *N.Espinoza*, Research Not. American Astron. Soc., **2**, 209, 2018. https://doi.org/10.3847/2515-5172/aaef38.
26. *D.M.Kipping*, Mon. Not. Roy. Astron. Soc., **435**, 2152, 2013. https://doi.org/10.1093/mnras/stt1435.
27. *J.S.Speagle*, Mon. Not. Roy. Astron. Soc., **493**, 3132, 2020. https://doi.org/10.1093/mnras/staa278.
28. *J.Skilling*, In: AIP Conference Proceedings, **735**, 395, 2004. https://doi.org/10.1063/1.1835238.
29. *K.F.Huber*, *S.Czesla*, *J.H.M.M.Schmitt*, Astron. Astrophys., **597**, A113, 2017. https://doi.org/10.1051/0004-6361/201629699.
30. *M.J.Holman*, *N.W.Murray*, Science, **307**(5713), 1288, 2005. https://doi.org/10.1126/science.1107822.
31. *M.Zechmeister*, *M.Kürster*, Astron. Astrophys., **496**, 577, 2009. https://doi.org/10.1051/0004-6361:200811296.
32. *J.-P.A.Zoghbi*, Publ. Astron. Soc. Australia, 28(3), 177, 2011. https://doi.org/10.1071/AS09062.
33. *A.Claret*, Astron. Astrophys., **600**, A30, 2017. https://doi.org/10.1051/0004-6361/201629705.